Rare Metal Materials and Engineering
Volume 53, Issue 5, May 2024
Available online at www.rmme.ac.cn

Science Press

Cite this article as: Yang Taisen, Zhang Guiqing, Dai Zhiyong, et al. Effect of In-situ Self-Generated MgO on Corrosion Resistance of KCl-$MgCl_2$ Molten Salt[J]. Rare Metal Materials and Engineering, 2024, 53(05): 1268-1276. DOI: 10.12442/j.issn.1002-185X.20230516.

ARTICLE

Effect of In-situ Self-Generated MgO on Corrosion Resistance of KCl-$MgCl_2$ Molten Salt

Yang Taisen, Zhang Guiqing, Dai Zhiyong, Liang Xuewei, Wang Yingdi, Su Yunhai

School of Materials Science and Engineering, Shenyang University of Technology, Shenyang 110870, China

Abstract: Molten chloride salt is excellent candidature for third-generation solar energy storage media due to its good energy storage advantages and low price. However, in the actual working environment, molten chloride salt has strong corrosion to metal pipes (Inconel 625 alloy). Inconel 625 welding wire is usually used as a repair material for solar pipeline. In order to solve the problem of strong corrosion of molten chloride salt to Inconel 625 cladding metal, Inconel 625 cladding metal was welded by MAG welding, and the effect of nano-MgO particles and $MgCl_2·6H_2O$ in-situ self-generated MgO on the corrosion of KCl-$MgCl_2$ molten salt was investigated. The results show that after 72 h of corrosion in KCl-$MgCl_2$, KCl-$MgCl_2$+5wt% MgO and KCl-$MgCl_2$+5wt% $MgCl_2·6H_2O$, the mass loss of Inconel 625 cladding metal is 0.00714, 0.00512, and 0.00308 $g·cm^{-2}$, respectively. The corrosion rate of Inconel 625 cladding metal in molten salt with in-situ self-generated MgO is decreased by 56.86% and 39.85%. Although the addition of nano-MgO particles in the molten salt can alleviate the corrosion of the chloride molten salt, the molten salt is agglomerated or settled, leading to a non-uniform distribution of MgO and $MgCr_2O_4$ protective shell layers. Adding $MgCl_2·6H_2O$ to the molten salt can generate in-situ MgO, and the generated MgO and $MgCr_2O_4$ protective shells are more uniform, which hinder the erosion of corrosive media, so it is an effective method to reduce the corrosion of chloride molten salt.

Key words: Inconel 625 cladding metal; chloride molten salt; in-situ self-generated MgO; corrosion inhibition

As an important material basis for human survival and development, fossil energy sources such as coal, oil and natural gas support the progress of human civilization and economy and social development. However, the mass consumption of fossil energy causes the emission of greenhouse gas (GHG), which increases the concentration of GHG in the atmosphere and enhances the greenhouse effect, leading to global warming. Meanwhile, a large number of toxic substances are emitted during the use of fossil energy[1–2]. At present, the development and utilization of stable, reliable and safe renewable energy have become the strategic choice of most countries in the world[3]. Solar energy is considered to be the most promising renewable energy, and concentrating solar power (CSP) has the highest conversion efficiency. Therefore, countries are developing solar power plants at a high speed[4].

Molten salt energy storage technology uses molten salt and other raw materials as heat transfer medium, which is combined with solar thermal power generation system to make the solar thermal power generation system has the ability to store energy and to generate electricity at night. The selection of the energy storage medium is very critical for next-generation CSP plants because it directly affects the efficiency of energy utilization and conversion in the energy storage system[5–6]. Gabriel[7] and Fernandez[8] et al have designed a non-eutectic mixed salt composed of 40wt% $NaNO_3$+60wt% KNO_3, which has been used as a "solar salt" in the second generation CSP power station. However, due to the thermal decomposition problem, its maximum operating temperature is limited to about 565 °C, which limits the heat storage temperature difference (ΔT) and the thermal storage capacity Q of the thermal storage system[9].

In recent years, in order to achieve further improvement in the operating efficiency of CSP and to reduce its operating cost, chloride molten salts have received much attention as energy storage media[10]. However, the chloride molten salt has strong corrosion resistance, which affects the long-term stability of the structure and properties of metal materials.

Received date: August 21, 2023
Corresponding author: Su Yunhai, Ph. D., Professor, School of Materials Science and Engineering, Shenyang University of Technology, Shenyang 110870, P. R. China, E-mail: su_yunhai@sut.edu.cn

When the energy storage pipeline is exposed to high-temperature chlorinated molten salt, it will encounter molten salt leakage accidents and reduce the life of the heat storage system[11–14]. Therefore, it is of great significance to take appropriate measures to reduce the corrosion of chlorinated molten salt for the stable operation of energy storage pipelines. In recent years, scholars have conducted in-depth research on methods to reduce the molten corrosion of chloride salts. Studies have shown that preventing direct exposure of structural metals to molten salts is the most effective method. In addition, some stable oxidation products generated on the metal surface can provide a beneficial effect[15]. As an example, Gomez-Vidal et al[16] formed an Al_2O_3 protective layer on the surface of Inconel 702, Haynes 224 and Kanthal APMT alloys by pre-oxidation. The dense and uniform Al_2O_3 shell protects the alloy from molten chloride corrosion. The corrosivity of chloride molten salt can also be reduced by changing the atmosphere of the corrosive environment. Rao et al[17] explored the corrosion of SS316L in $NaCl/Na_2CO_3$ molten salt under air and argon environments. The results indicate that the molten salt corrosion is linked to the amount of oxygen, and the argon environment can reduce the corrosion of molten salt, because the solubility of alloying elements is large due to the high content of oxygen in the air environment, while in the argon environment, a layer of Cr_2O_3 is generated on the surface of the specimen. The corrosiveness of molten salts is also related to the experimental temperature. Wang et al[18] investigated the corrosion of 316 stainless steel and Inconel 625 alloy submerged in NaCl-KCl-$ZnCl_2$ molten salt at 700 and 900 °C. The results indicate that both alloys display reactive corrosion in chloride molten salts. With the increase in temperature, the corrosion rate is increased. In addition, the addition of corrosion inhibitors to molten salts is also considered as an effectively corrosion protection method. The addition of corrosion inhibitor can remove all kinds of impurities in the molten salt (such as transition metal ions, dissolved O_2 or Cl_2, H_2O, hydrolysis products HCl, MgOHCl, etc), and play a purification effect on the molten salt. Fernandez[19] reduced the corrosion current density of HT700 alloy in chloride molten salt by adding Al, which reacted with the impurities on the surface of the alloy to form an Al_2O_3 layer, and the beneficial effect of Al increased with the increase in Al content in chloride molten salt. At the same time, the incorporation of Al hindered the diffusion of the Cr element to the outside, thus prolonging the life of the HT700 alloy in chloride molten salts. In addition, Ding et al[20] explored the effect of Mg treatment on the corrosion of molten NaCl-KCl-$MgCl_2$ salts. The results indicate that Mg treatment removes the corrosive impurities HCl and MgOHCl in the molten salt and reduces the corrosivity of the salt.

In addition, the addition of nanoparticles to chloride molten salt can form a tight adsorption layer on the surface of the molten salt, which not only mitigates the corrosive properties of the molten salt, but also improves its thermal storage properties, thus being a better corrosion protection strategy. The study of Wei et al[21] showed that the addition of 5.0wt% MgO particles to the chloride molten salt can effectively increase the heat transfer performance of the molten salt, and MgO reduces alloy corrosion when it is deposited on the surface of Inconel 625 alloy. At present, the corrosion inhibition technology of chloride molten salt is mainly aimed at casting alloys. However, due to the space constraints in the solar heat storage tube, in the event of corrosion failure, Inconel 625 flux-cored wire is often used to repair[22]. The corrosion inhibition technology of repairing Inconel 625 cladding metal is rarely reported.

Based on the anti-corrosion technology of nano-MgO particles, a method of in-situ generation of MgO was proposed in this study, which can further reduce the corrosion degree of Inconel 625 cladding metal in KCl-$MgCl_2$ molten salt. According to Yang's research[15], it is known that the corrosion loss of Inconel 625 cladding metal in KCl-$MgCl_2$ (60mol%–40mol%) molten salts is the minimal. Therefore, in this study, KCl-$MgCl_2$ (60mol%–40mol%) molten salt was chosen as the basis. The corrosion behavior of Inconel 625 cladding metal in KCl-$MgCl_2$, KCl-$MgCl_2$+5wt% MgO and KCl-$MgCl_2$+5wt% $MgCl_2·6H_2O$ at 600 °C was investigated. The corrosion mass loss and corrosion rate of Inconel 625 cladding metal were calculated by mass loss method, and the corrosion products, surface morphology and cross-section morphology were analyzed to explore the corrosion inhibition mechanism. The research results are expected to provide a reference for the development of corrosion inhibition technology after repair of energy storage tubes in solar power plants.

1 Experiment

1.1 Preparation of mixed salt

The binary phase diagram of KCl-$MgCl_2$ was calculated by Fact Sage software, as shown in Fig.1. It can be seen that KCl-$MgCl_2$ is in a molten state at 600 °C, so the effect of temperature on the molten salt is excluded. KCl, $MgCl_2$ and $MgCl_2·6H_2O$ were all A. R. grade (purity>99.7%), and MgO particles with diameter of 50 nm were purchased from Shanghai McLean Biochemical Co., Ltd. Before the experiment, all the corrosive salts were dried in a vacuum oven at 200 °C for 24 h. After drying, the corrosive salt was placed in a glove box filled with Ar atmosphere for weighing.

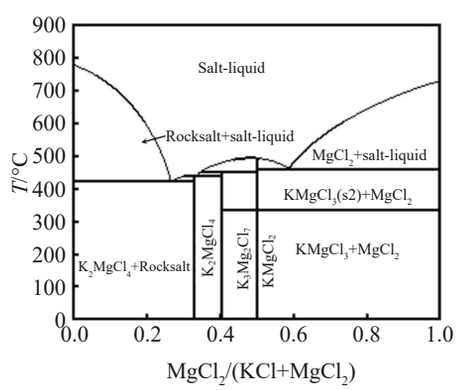

Fig.1 KCl-$MgCl_2$ binary molten salt phase diagram

The preparation process of KCl-$MgCl_2$ (60mol%–40mol%) and KCl-$MgCl_2$ (60mol%–40mol%)+5wt% MgO mixed salts was as follows: the corrosive salts were ground and mixed evenly in a glove box, and then placed in an alumina crucible with a lid. The corrosion experiments were conducted in a box-type resistance furnace with the heating rate of 5 °C/min. The furnace was heated to 600 °C and held for 4 h. Finally, the mixed salt was cooled to room in a vacuum drying oven.

$MgCl_2·6H_2O$ reacted at a specific temperature to form MgOHCl, which was decomposed into MgO at 533–568 °C, as shown in Eq. (1–7) [23]. The mixed salt containing 5wt% $MgCl_2·6H_2O$ was placed in a resistance furnace and the heating rate was set to 5 °C/min. Firstly, the resistance furnace was heated to 350 °C and held for 2 h, so that $MgCl_2·6H_2O$ completely reacted to form MgOHCl. Finally, the resistance furnace was heated to 600 °C and held for 4 h to decompose MgOHCl into MgO. By controlling the reaction conditions, MgO was formed in-situ in the mixed salt containing 5wt% $MgCl_2·6H_2O$.

$$MgCl_2·6H_2O = MgCl_2·4H_2O + 2H_2O \quad 96-117\ ℃ \tag{1}$$

$$MgCl_2·4H_2O = MgCl_2·2H_2O + 2H_2O \quad 107-180\ ℃ \tag{2}$$

$$MgCl_2·2H_2O = MgCl_2·H_2O + H_2O \quad 153-242\ ℃ \tag{3}$$

$$MgCl_2·H_2O = MgCl_2 + H_2O \quad 307-400\ ℃ \tag{4}$$

$$MgCl_2·2H_2O = MgOHCl + HCl(g) + H_2O \quad 193-240\ ℃ \tag{5}$$

$$MgCl_2 + H_2O = MgOHCl + HCl(g) \quad 210-445\ ℃ \tag{6}$$

$$MgOHCl = MgO + HCl(g) \quad 533-568\ ℃ \tag{7}$$

Inconel 625 flux-cored wire has outstanding corrosion resistance and moderate price. It has been widely used in practice as the best choice for repairing solar energy storage pipelines. In this study, Inconel 625 flux-cored wire provided by Tiantai Welding Materials Industry Co., Ltd (composition is shown in Table 1) was used. Inconel 625 cladding metal was prepared by MAG welding. The welding parameters are as follows: welding current 150 A, welding voltage 24 V, welding speed 250 mm/min, and shielding gas 80vol% Ar+20vol% CO_2. The Inconel 625 cladding metal with a thickness of 12 mm was prepared by depositing the welding wire on the Q235 substrate. Because the interlayer temperature has a large impact on the surfacing, the interlayer temperature was strictly controlled as ≤120 °C in the welding process. In the welding process, the dilution rate makes the metal elements in the base metal and the surfacing layer diffuse to each other, which affects the performance. For avoiding the effect of dilution rate on the corrosion resistance of samples, the total 4 layers were welded. High-temperature molten salt corrosion specimens were taken from layers 2 and 3 of the cladding layer. The schematic diagram is shown in Fig. 2. The size of Inconel 625 cladding metal corrosion sample was 10 mm×10 mm×2 mm. In view of removing the oxide film on the surface

Table 1 Chemical composition of Inconel 625 welding wire (wt%)

Cr	Mo	Mn	Fe	Si	Ti	P	S	Ni
21.2	8.6	0.23	0.9	0.43	0.16	0.01	0.006	Bal.

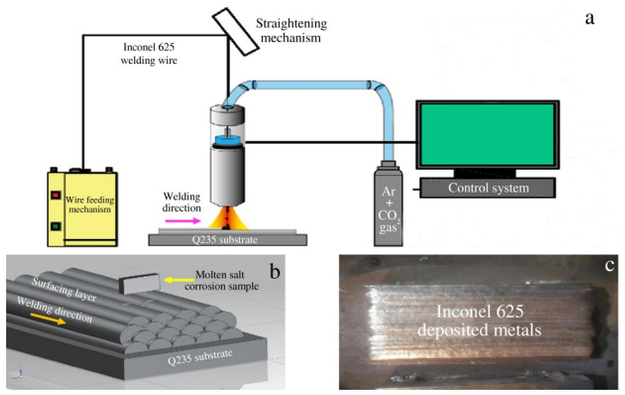

Fig.2 Schematic diagram of Inconel 625 cladding metal preparation: (a) welding, (b) pickup, and (c) appearance of Inconel 625 cladding metal

of the corrosion specimen and obtaining a smooth surface, it was firstly sanded and burnished with diamond sandpaper and subsequently removed by washing with acetone in an ultrasonic water bath to remove residual impurities. Each specimen was weighed with an e-balance of 0.0001 g in accuracy. To keep the data accurate, three samples were placed in each group of tests and the test results were averaged.

1.2 Method

The steps for the three sets of corrosion experiments were the same. Taking the KCl-$MgCl_2$ molten salt corrosion experiment as an example, the crucible was cleaned and dried with deionized water and alcohol. The Inconel 625 cladding metal corrosion sample was placed horizontally in the preheated crucible. Next, the corrosive salts were weighed to achieve the required proportion (40mol% $MgCl_2$+60mol% KCl), uniformly mixed and dried in a vacuum drying oven at 120 °C for 24 h. In order to ensure the accuracy of the data, three Inconel 625 cladding metal corrosion samples were placed in each group of experiments, and the samples were placed horizontally in an alumina crucible. The homogeneous corrosion salt was poured into an alumina crucible and then transferred to the high temperature furnace. It is important that the crucible was sealed with a lid to isolate the O_2 and H_2O. The corroded samples were immersed for 72 h. The corroded samples were placed in a drying oven under vacuum. After the sample was cooled, the residual salt on the surface was removed by ultrasonic vibration.

The mass loss was calculated by Eq.(8) [24]:

$$\Delta m/S_0 = (m_f - m_i)/S_0 \tag{8}$$

where Δm represents the mass loss of Inconel 625 cladding metal (g); m_f is the initial mass of the sample (g); m_i is the mass of the sample after corrosion (g); S_0 is the initial surface area of the sample (cm^2).

The corrosion rate v ($\mu m·a^{-1}$) was calculated by Eq.(9) [25]:

$$v = 365 \times 10000\,[\Delta m/(\rho ST)] \tag{9}$$

where ρ is the density of Inconel 625 cladding metal ($g·cm^{-3}$), S is the immersion area (cm^2) of Inconel 625 cladding metal,

and T is the corrosion time (h).

The surface and cross-sectional morphology of Inconel 625 cladding metal corrosion samples were detected by scanning electron microscope (SEM, Gemini 300), and the element distribution was analyzed by energy disperse spectroscopy (EDS). The corrosion products on the surface of the sample were measured by X-ray diffractometer (XRD-7000, pure Cu target, voltage 40 KV, current 30 mA, step size 2°/min, scanning range 20°–90°). X-ray photoelectron spectroscopy (XPS) with Thermo Scientific ESCALAB Xi+ was used to measure the element bonding and valence state information in the corrosion film of Inconel 625 cladding metal under different corrosion conditions, and assisted other measurement methods to analyze the structural composition of the corrosion film. XPS used a monochromatic Al Kα ray source as the excitation light source (energy: 1486.6 eV). The measurement step was 0.05 eV.

2 Results and Discussion

2.1 Thermodynamic analysis of corrosion process

When there are other impurities in the molten salt (such as O_2 and H_2O), the chloride molten salt exhibits strong corrosivity due to the synergistic effect. These impurities react with Cl^- at high temperatures to form corrosive products such as Cl_2 and HCl, as shown in Eq. (10–11):

$$O_2(g)+4Cl^-=2O^{2-}+2Cl_2(g) \quad (10)$$

$$H_2O(g)+2Cl^-=O^{2-}+2HCl(g) \quad (11)$$

In the molten salt corrosion, the Cr element in the Inconel 625 cladding metal is more active than the Ni element, so the Cr element is preferentially dissolved[26]. The dissolved elements react to form oxides such as Cr_2O_3 and NiO, but Cr_2O_3 and NiO are unstable and continuously react to form looser corrosion products such as $NiCr_2O_4$, as shown in Eq.(12) [27].

$$NiO(s)+Cr_2O_3(s)=NiCr_2O_4(s) \quad (12)$$

Since the molten salt contains $MgCl_2$, the presence of H_2O in the impurities leads to the hydrolysis of $MgCl_2$ into MgO. Part of MgO further reacts with Cr_2O_3 to form $MgCr_2O_4$, as shown in Eq.(13–14):

$$MgCl_2(l)+H_2O(g)=MgO(s)+2HCl(g) \quad (13)$$

$$Cr_2O_3(s)+MgO(s)=MgCr_2O_4(s) \quad (14)$$

Activation-oxidation is an important mechanism of metal molten salt corrosion[18]. $CrCl_4$ (g) is formed during the corrosion process, which results in large loss of Cr due to diffusion, as shown in Eq.(15–16)[28–29]:

$$Cr(s)+2Cl_2(g)=CrCl_4(g) \quad (15)$$

$$Cr(s)+2MgCl_2(l)+O_2(g)=CrCl_4(g)+2MgO(s) \quad (16)$$

As shown in Eq. (17), $CrCl_4$ reacts with MgO to form $MgCr_2O_4$ at high temperature[30]. According to Ref. [30], the relatively dense structure of $MgCr_2O_4$ and MgO prevents the corrosion of metals from chloride molten salts.

$$2CrCl_4(g)+2MgO(s)=MgCr_2O_4(s)+3MgCl_2(l)+Cl_2(g) \quad (17)$$

2.2 Corrosion dynamics and corrosion rate curve

After corrosion of Inconel 625 cladding metal in three different chloride molten salts for 72 h, the corrosion mass loss and corrosion rate results of the sample are shown in Fig.3. In all three molten salts, the loss of quality is gradually increased with the corrosion time. The mass loss in the KCl-$MgCl_2$ molten salt is mainly caused by solubilization of metal oxides and erosion by corrosive products. Although Cr_2O_3 has beneficial effect, it is weakly characterized by poor stability in chloride molten salts and gradually dissolved[31]. The leftover NiO after Cr_2O_3 is soluble with a bone structure that promotes the buildup of O_2, H_2O and other impurities, leading to more severe corrosion behavior[31]. It is deduced that Cr_2O_3 and other oxides are not completely solubilized during the beginning stages of corrosion, which has a beneficial effect on the Inconel 625 cladding metal. However, with the dissolution of Cr_2O_3, the beneficial effect of the protective layer on the cladding metal is reduced. As a result, the corrosion loss of the Inconel 625 cladding metal grows slowly in the early stages and increases sharply in the later stages.

After 72 h of corrosion in KCl-$MgCl_2$, KCl-MgCl-MgO and KCl-$MgCl_2$-$MgCl_2{\cdot}6H_2O$, the mass loss of Inconel 625 cladding metal is 0.00714, 0.00512 and 0.00308 g·cm^{-2}, respectively. KCl-$MgCl_2$-$MgCl_2{\cdot}6H_2O$ molten salt has the lowest corrosion effect.

2.3 Characterization of MgO composite chloride molten salt

Fig. 4 shows the surface morphology and element distribution of MgO in composite chloride molten salt. It can be seen that the nano-MgO added in the molten salt is not distributed evenly and the size of the grains varies greatly. The

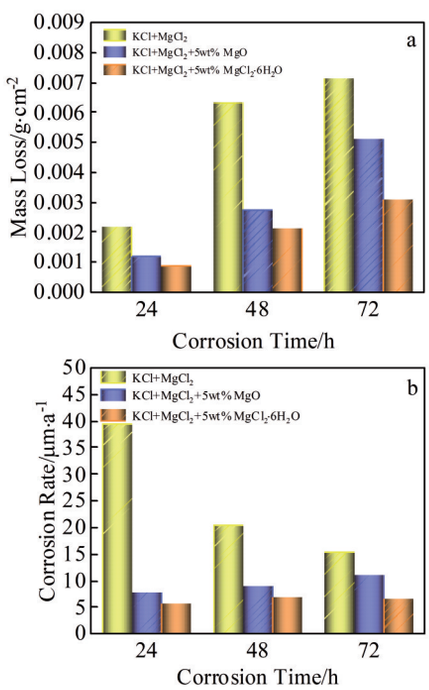

Fig.3 Corrosion mass loss (a) and corrosion rate (b) results of Inconel 625 cladding metal in three molten salts

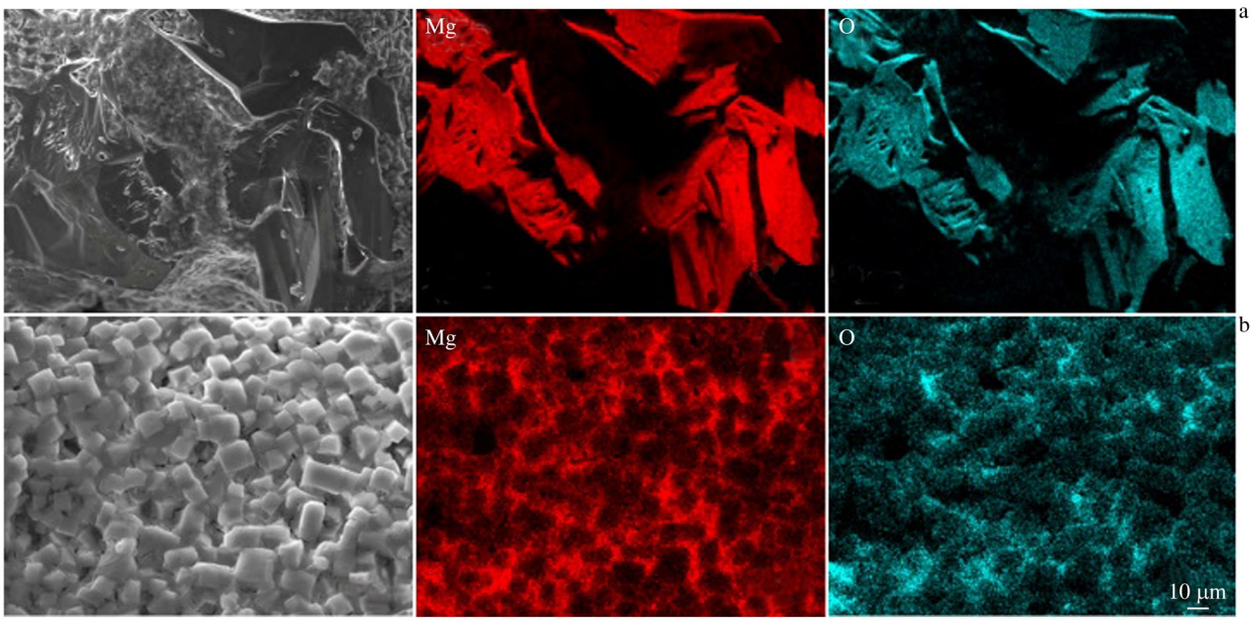

Fig.4 Surface morphologies and element distributions of composite chloride molten salts: (a) KCl-$MgCl_2$-MgO and (b) KCl-$MgCl_2$-$MgCl_2 \cdot 6H_2O$

in-situ generated MgO particles are uniformly distributed in the molten salt.

2.4 Surface analysis of sample after corrosion

The corrosion samples of Inconel 625 cladding metal are corroded at 600 °C for 72 h, and then tested by XRD. The results are shown in Fig. 5. Cr0.19Fe0.7Ni0.11 phase is detected on the surface of the sample. MgO, $MgCr_2O_4$ and $NiCr_2O_4$ corrosion products are observed on the sample surface in KCl-$MgCl_2$ salt. However, no Cr_2O_3 is detected. It shows that Cr_2O_3 is an intermediate product, which is easier to react with MgO than other oxides. XRD results of the samples in KCl-$MgCl_2$-MgO and KCl-$MgCl_2$-$MgCl_2 \cdot 6H_2O$ molten salts show that Cr0.19Fe0.7Ni0.11, MgO, $MgCr_2O_4$ and $NiCr_2O_4$ corrosion products are detected.

At 600 °C, the surface morphologies of Inconel 625 cladding metal after corrosion in three molten salts for 72 h are shown in Fig. 6. Fig. 6a shows the surface morphology of the sample after corrosion in KCl-$MgCl_2$ molten salt for 72 h.

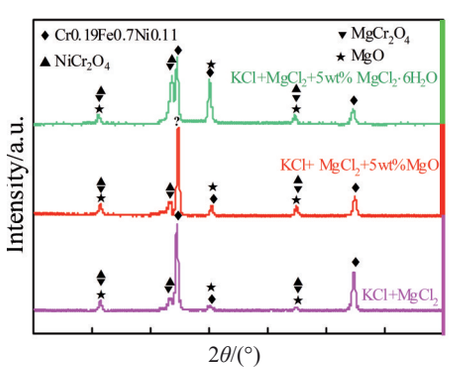

Fig.5 XRD patterns of the sample surface after corrosion in three molten salts at 600 °C for 72 h

The distribution of corrosion products on the surface of Inconel 625 cladding metal is not even, and corrosion pores appear on the surface of the cladding metal. These corrosion pores are connected to each other to form corrosion passages. Corrosion pores and passages are induced by the outward propagation of gaseous metal chlorides resulting from high temperatures. As the corrosion reaction progresses, the corrosion products gradually penetrate the Inconel 625 cladding metal matrix and gradually occupy the position of the metal element, resulting in serious corrosion[32]. According to the XRD results and the element distributions in Fig. 6a, MgO and $MgCr_2O_4$ form on the surface of Inconel 625 cladding metal. However, the MgO and $MgCr_2O_4$ shell layers are not uniformly distributed, indicating that the hydrolysis of $MgCl_2$ is not uniform.

Fig. 6b shows the surface morphology and element distributions of Inconel 625 cladding metal after corrosion in molten KCl-$MgCl_2$-MgO salt for 72 h. It can be seen that the distribution of Mg element is not uniform. In conjunction with the XRD results and the elemental assignments in Fig. 6b, it is deduced that the right side is MgO and $MgCr_2O_4$ shell layers, which have a favorably protective role, and thus the corrosion in this region is relatively lighter. The distribution of Cr element on the surface of Inconel 625 cladding metal is not uniform, suggesting severe corrosion of the cladding metal without shell layer protection, and Cr element is lost in large quantities. This indicates that the added MgO cannot be uniformly mixed in the chloride molten salt, and the phenomenon of agglomeration and sedimentation of MgO occurs[33–34]. Fig. 6c shows the surface morphology of Inconel 625 cladding metal after corrosion in KCl-$MgCl_2$-$MgCl_2 \cdot 6H_2O$ molten salt for 72 h. Compared with the surface morphologies in Fig. 6a–6b, the surface is more flat and the element distribution is

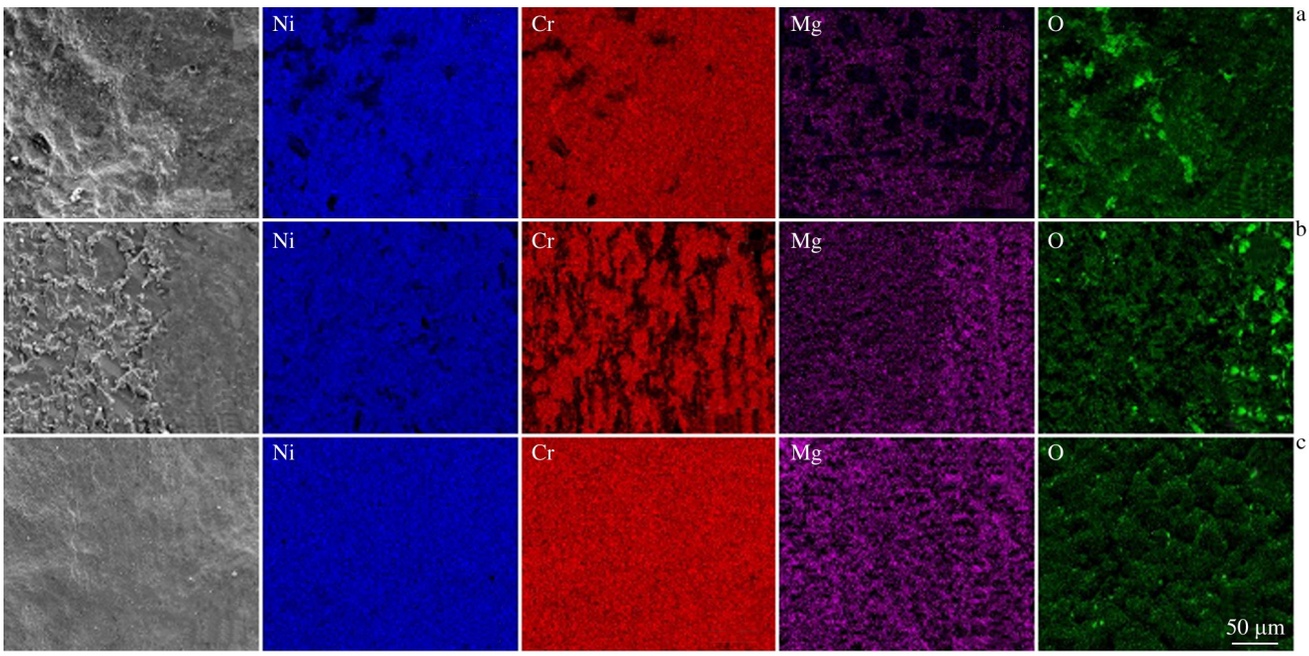

Fig.6 Surface morphologies and element distributions of Inconel 625 cladding metal after corrosion in different chloride molten salts at 600 °C for 72 h: (a) KCl-$MgCl_2$, (b) KCl-$MgCl_2$-MgO, and (c) KCl-$MgCl_2$-$MgCl_2 \cdot 6H_2O$

uniform. Combined with the XRD results, the in-situ generated MgO in the molten KCl-$MgCl_2$ salt homogeneously spreads. The protective layer formed by corrosion products such as MgO and $MgCr_2O_4$ is complete and dense. They are evenly distributed on the surface of the sample, so they play a better protective role.

In order to further analyze the elemental composition and chemical state of surface corrosion products of Inconel 625 cladding metal under different molten salt conditions, the Inconel 625 cladding metal is characterized by XPS, and the results are shown in Fig. 7. According to the high resolution spectra of XPS, it can be seen that the signals of Cr, Ni, O and Mg on the surface of the samples in different molten salt systems are strong. This indicates that the corrosion products on the surface of the sample are mainly compounds consisting of Cr, Ni, Mg and O, as shown in Fig.7a–7c. The Ni 2p orbital is divided into four peaks. After consulting the Avantage software database, 854.12 and 873.94 eV correspond to $NiCr_2O_4$, and 860.93 and 877.82 eV are companion peaks. According to the high-resolution XPS spectrum of Cr 2p and the Avantage software database, 577.03 eV corresponds to $NiCr_2O_4$ and 586.8 eV corresponds to $MgCr_2O_4$. Similarly, 1304.25 eV in the high-resolution XPS spectrum of Mg 2p corresponds to MgO. In the XPS spectrum of O 1s, 529.51 eV is the characteristic peak of M-O compound. Combining the results of XRD and XPS, it is seen that the corrosion products on the surface of Inconel 625 cladding metal after corrosion under different molten salt conditions are mainly composed of MgO, $NiCr_2O_4$ and $MgCr_2O_4$. From the peak area of MgO in XPS results, we know that under the condition of KCl-$MgCl_2$-$MgCl_2 \cdot 6H_2O$ molten salt, Inconel 625 cladding metal generates more MgO and $MgCr_2O_4$, which have a beneficial effect. Thus, the corrosion resistance of Inconel 625 cladding metal is improved. This is consistent with the surface element distribution results of the above Inconel 625 cladding metal.

2.5 Cross section analysis

The cross-sectional morphologies of Inconel 625 cladding metal after corrosion in three molten salts at 600 °C for 72 h are shown in Fig. 8. The cross-section is split into three parts from the external to the internal: the outer corrosion layer, the inner corrosion layer and the cladding metal substrate. The outer corrosion layer consists of a wide range of corrosion products, and the inner corrosion layer is the part where elements are lost. The thickness of the corrosion layer is the largest in KCl-$MgCl_2$ molten salt, which is 39.17 μm. In the KCl-$MgCl_2$-MgO molten salt, the thickness of the corrosion layer of the sample is reduced to 35.23 μm. The lowest corrosion layer thickness of the sample is 31.58 μm in KCl-$MgCl_2$-$MgCl_2 \cdot 6H_2O$ molten salt. The outer corrosion layer and the inner corrosion layer are only 16.21 and 15.37 μm in thickness, respectively. In terms of the thickness of the corrosion layer, the molten KCl-$MgCl_2$-$MgCl_2 \cdot 6H_2O$ salt has the lowest corrosivity among the three molten salts.

Fig. 9 shows the cross-sectional element distributions of Inconel 625 cladding metal after corrosion at 600 °C for 72 h. Fig. 9a and 9b show that the distribution of Mg element is not uniform, and the diffusion of Cr element is serious. Fig. 9c shows the cross-sectional element distribution of Inconel 625 cladding metal after corrosion in KCl-$MgCl_2$-$MgCl_2 \cdot 6H_2O$ molten salt for 72 h. The external corrosion layer is mainly made up of MgO and $MgCr_2O_4$, and the structure is dense and evenly covers the surface of the

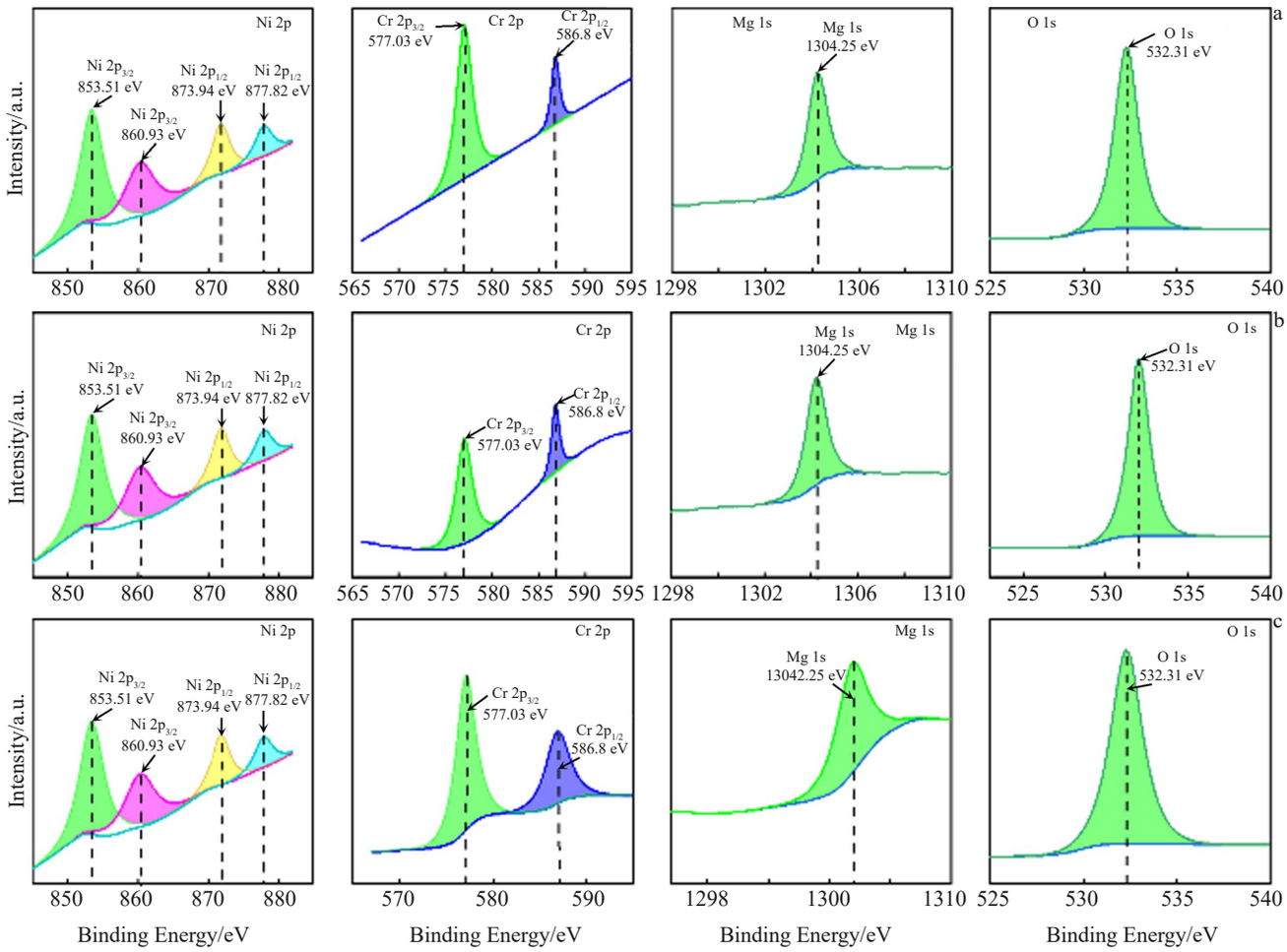

Fig.7 XPS spectra of the surface of Inconel 625 cladding metal after corrosion under different molten salt conditions: (a) KCl-$MgCl_2$, (b) KCl-$MgCl_2$-MgO, and (c) KCl-$MgCl_2$-$MgCl_2 \cdot 6H_2O$

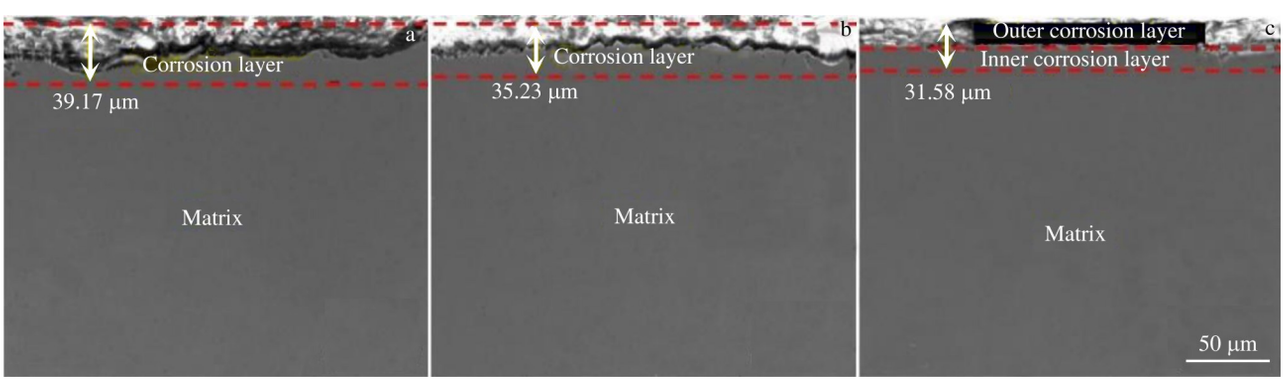

Fig.8 Cross-sectional morphologies of Inconel 625 cladding metal after corrosion at 600 °C for 72 h: (a) KCl-$MgCl_2$, (b) KCl-$MgCl_2$-MgO, and (c) KCl-$MgCl_2$-$MgCl_2 \cdot 6H_2O$

cladding metal. The external corrosion layer is closely combined with the cladding metal matrix and has a good beneficial effect[35]. The elements are evenly distributed during the corrosion process. Combined with Fig. 9c, it is seen that the corrosion channel of Inconel 625 cladding metal is not obvious. The explanation for this is the gradual thickening of the dense MgO and $MgCr_2O_4$ shell layers as the corrosion process continues, which hinders the erosion of corrosive media. Therefore, it is concluded that the corrosion effect of KCl-$MgCl_2$-$MgCl_2 \cdot 6H_2O$ molten salt is lower than that of other salts. Fig. 10a and Fig. 10b display the conservation effect of the corrosion layer

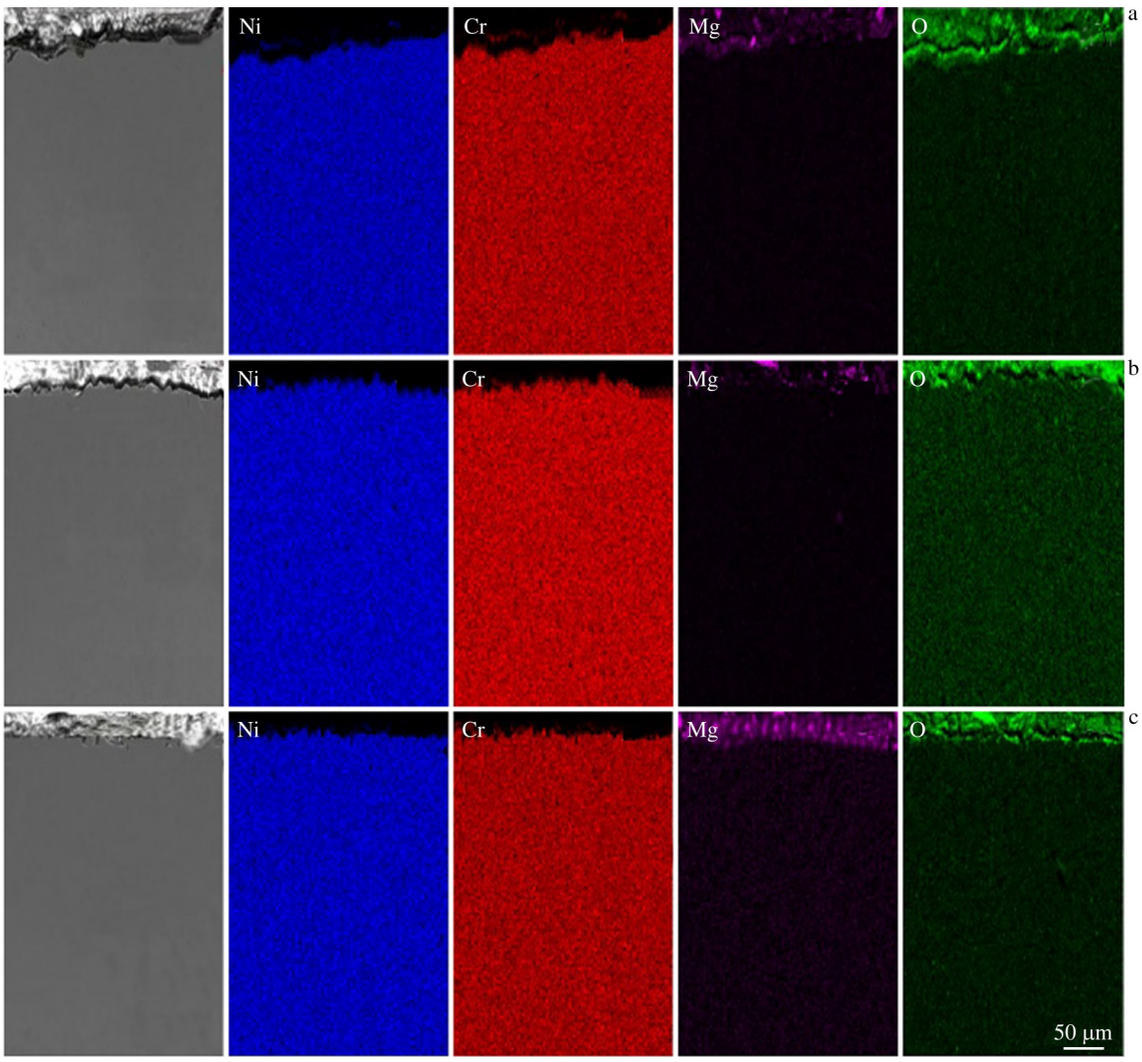

Fig.9 Cross-sectional element distributions of Inconel 625 cladding metal after corrosion in different chloride molten salts at 600 °C for 72 h: (a) KCl-$MgCl_2$, (b) KCl-$MgCl_2$-MgO, and (c) KCl-$MgCl_2$-$MgCl_2 \cdot 6H_2O$

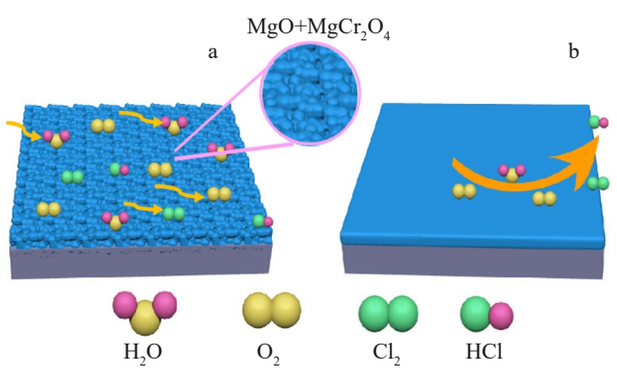

Fig.10 Conservation effect of corrosion layer formed by Inconel 625 cladding metal in different molten salts: (a) KCl-$MgCl_2$-MgO and (b) KCl-$MgCl_2$-$MgCl_2 \cdot 6H_2O$

formed by Inconel 625 cladding metal in KCl-$MgCl_2$-MgO and KCl-$MgCl_2$-$MgCl_2 \cdot 6H_2O$ molten salts, respectively.

3 Conclusions

1) The corrosion effect of KCl-$MgCl_2$+5wt% $MgCl_2 \cdot 6H_2O$ molten salt is lower than that of KCl-$MgCl_2$ and KCl-$MgCl_2$+5wt% MgO molten salts, in which the corrosion depth of Inconel 625 cladding metal at 600 °C is 39.17, 35.23 and 31.58 μm, respectively. In-situ MgO can reduce the corrosion of KCl-$MgCl_2$ molten salt.

2) In KCl-$MgCl_2$+5wt% MgO molten salt, the added MgO particles are not uniformly dispersed, and agglomeration or sedimentation occurs. This leads to the formation of MgO and $MgCr_2O_4$ shells in some areas of Inconel 625 cladding metal surface. Therefore, different areas on the surface of the sample have different corrosion conditions.

3) In KCl-$MgCl_2$+5wt% $MgCl_2 \cdot 6H_2O$ molten salt, the in-situ self-generated MgO particles are uniformly dispersed. During the corrosion process, the protective layer formed by corrosion products such as MgO and $MgCr_2O_4$ is complete and dense, and the corrosion products are evenly distributed on the surface of the sample, playing a better

protective role. Therefore, in-situ formation of MgO is an effective strategy to reduce the corrosion effect of KCl-$MgCl_2$ molten salt.

References

1 Kumar K R, Chaitanya N V V K, Kumar N S. *Journal of Cleaner Production*[J], 2021, 282: 125296
2 Haviv S, Revivo N, Kruger N *et al. ACS Applied Materials & Interfaces*[J], 2020, 12: 36040
3 Pata U K. *Renewable Energy*[J], 2021, 173: 197
4 Yuan L, Zhu Q, Zhang T *et al. Renewable Energy*[J], 2021, 169: 1121
5 Prieto C, Cooper P, Ines Fernandez A *et al. Renewable & Sustainable Energy Reviews*[J], 2016, 60: 909
6 Guillot S, Faik A, Rakhmatullin A *et al. Applied Energy*[J], 2012, 94: 174
7 Gabriel Z, Solé A, Camila B *et al. Energies*[J], 2018, 11(9): 2358
8 Fernandez A G, Cabeza L F. *Journal of Energy Storage*[J], 2020, 27: 101125
9 Liu T, Xu X, Liu W *et al. Solar Energy*[J], 2019, 191: 435
10 Liu M, Tay N H S, Bell S *et al. Renewable & Sustainable Energy Reviews*[J], 2016, 53: 1411
11 D'Souza B, Zhuo W, Yang Q *et al. Corrosion Science*[J], 2021, 187: 109483
12 D'Souza B, Leong A, Yang Q *et al. Corrosion Science*[J], 2021, 182: 109285
13 Vignarooban K, Xu X H, Wang K *et al. Applied Energy*[J], 2015, 159: 206
14 Gonzalo A P, Marugán A P, Márquez F P G. *Applied Energy*[J], 2019, 255: 113893
15 Yang T, Su Y, Liu H *et al. Materials Research Express*[J], 2020, 7(12): 126505
16 Gomez-Vidal J C, Fernandez A G, Tirawat R *et al. Colar Energy Materials and Solar Cells*[J], 2017, 166: 222
17 Rao C J, Shankar A R, Ajikumar P K *et al. Corrosion*[J], 2015, 71(4): 502
18 Wang M, Zeng S, Zhang H *et al. High Temperature Materials and Processes*[J], 2020, 39(1): 340
19 Fernandez A G, Cabeza L F. *Applied Sciences*[J], 2020, 10(11): 3724
20 Ding W J, Shi A, Jian Y L *et al. Solar Energy Materials and Solar Cells*[J], 2019, 193: 298
21 Wei X, Song M, Wang W *et al. Applied Energy*[J], 2015, 156: 306
22 Zhang Zhongke, Xiong Jianqiang, Chu Shusheng *et al. Rare Metal Materials and Engineering*[J], 2023, 52(5): 1842 (in Chinese)
23 Zhao Y V J. *Solar Energy Materials and Solar Cells*[J], 2020, 215: 110663
24 Fernandez A G, Perez F J. *Solar Energy*[J], 2016, 134(9): 468
25 Soleimani D A, Durham R N, Galetz M C. *Solar Energy Materials & Solar Cells*[J], 2016, 144: 109
26 Chen Shanshan, Liu Zongde, Pan Chaoyang *et al. Rare Metal Materials and Engineering*[J], 2023, 52(8): 2702
27 Grégoire B, Oskay C, Meiner T M *et al. Solar Energy Materials and Solar Cells*[J], 2020, 215: 110659
28 Fernández A G, Cabeza L F. *Journal of Energy Storage*[J], 2020, 29: 101381
29 Li Xiaoya, Zou Jianpeng, Shi Qian *et al. Rare Metal Materials and Engineering*[J], 2022, 51(11): 3989
30 Liu B, Wei X, Wang W *et al. Solar Energy Materials and Solar Cells*[J], 2017, 170: 77
31 Ishitsuka T, Nose K. *Materials & Corrosion*[J], 2000, 51(3): 177
32 Liu Q, Wang Z R. Liu W H *et al. Corrosion Science*[J], 2021, 180: 109183
33 Nithiyanantham U, Grosu Y, Gonzalez-Fernandez L *et al. Solar Energy*[J], 2019, 189(9): 219
34 Fernández A G, Muoz-Sánchez B, Nieto-Maestre J *et al. Renewable Energy*[J], 2019, 130: 902
35 He X, Robb K R, Sulejmanovic D *et al. ACS Sustainable Chemistry & Engineering*[J], 2021, 9(14): 4941

原位自生 MgO 对氯化物熔盐腐蚀性的影响

杨太森，张桂清，戴志勇，梁学伟，王英第，苏允海

(沈阳工业大学 材料科学与工程学院，辽宁 沈阳 110870)

摘　要：熔融氯化物盐是优异的传热流体和热能储存介质，在太阳能发电领域具有广泛的应用价值。但在实际工作环境下，熔融氯化物盐对金属管道（Inconel 625合金）有较强的腐蚀性，Inconel 625焊丝通常作为修补材料在太阳能管道修补上使用。为了解决熔融氯化物盐对Inconel 625熔敷金属的强腐蚀性问题，采用MAG焊堆焊出Inconel 625熔敷金属，探究在KCl-$MgCl_2$熔盐中加入纳米级MgO颗粒与$MgCl_2·6H_2O$原位自生MgO对KCl-$MgCl_2$盐腐蚀性的影响。结果表明：Inconel 625熔敷金属在KCl-$MgCl_2$、KCl-$MgCl_2$+5% MgO和KCl-$MgCl_2$+5% $MgCl_2·6H_2O$（质量分数）中经过72 h的腐蚀后，试样的质量损失分别为0.00714、0.00512和0.00308 $g·cm^{-2}$。Inconel 625熔敷金属在原位自生MgO熔盐中的腐蚀速率同比降低56.86%和39.85%。熔盐中加入纳米MgO颗粒虽然能够缓解氯化物熔盐的腐蚀性，但熔盐发生团聚或沉降现象，导致MgO和$MgCr_2O_4$保护壳层分布不均匀；在熔盐中添加$MgCl_2·6H_2O$使其原位生成MgO，生成的MgO和$MgCr_2O_4$保护壳层更加均匀，能够阻碍腐蚀性介质侵蚀，是降低氯化物熔盐腐蚀性的有效方法。

关键词：Inconel 625熔敷金属；氯化物熔盐；原位自生MgO；缓蚀

作者简介：杨太森，男，1995年生，博士生，沈阳工业大学材料科学与工程学院，辽宁 沈阳 110870，E-mail：yangtaisen19950421@163.com